International Journal of Creative and Open Research in Engineering and Management
ISSN: **3108-1754 (Online)**
Volume 02 Issue 08 August-2026 | Impact Factor: 3.5

Incipient Fault Diagnosis of Cylindrical Roller Bearings Using Dynamic Response Analysis

Umakant Banswarti, Shashikant Pandey
Department of Mechanical Engineering, Eklavya University, Damoh

How to Cite this Article:

Banswarti, Umakant, and Shashikant Pandey. "Incipient Fault Diagnosis of Cylindrical Roller Bearings Using Dynamic Response Analysis." International Journal of Creative and Open Research in Engineering and Management 02, no. 8 (2026): 1-18. https://doi.org/10.55041/ijcope.v2i8.254.

https://doi.org/10.55041/ijcope.v2i8.254

Abstract

Detecting faults early on is important in order to maintain the health of rotating machinery. Incipient faults in rolling-element bearings lead to the generation of micro-defects which create weak transient impact signals. However, these are often buried within the background vibration of the machine and structural transmission effects. Indicators based on traditional time-domain methods possess sensitivity to impulsive damage, but when the signal exhibits non-stationarity or a noisy trend. The current study compares time-domain statistical parameters and FFT spectral analysis for progressive inner race damage in an NJ307 cylindrical roller bearing. A wire electrical-discharge-machining technique produces artificial inner-race defects with sizes of 0.25 mm, 0.50 mm, 0.75 mm and 1.00 mm, while a healthy bearing serves as the reference condition. Vibration is measured with a single-axis accelerometer connected to an eight-channel Dewesoft data-acquisition system with a sampling frequency of 20 kHz; the shaft speed is 800 rpm by use of a variable-frequency drive.

The RMS, standard deviation, peak value, crest factor, kurtosis, and form factor are taken into account during the analysis. FFT spectra are observed at the calculated inner-race fault frequency and its harmonics. The findings reveal that at the earliest damage stage, there is only a gradual change in both RMS and standard deviation. In contrast, changes in peak value, crest factor, kurtosis, and amplitudes of the BPFI-related FFT are more robust indicators of progressive damage. The FFT provides statistically interpretable frequency information, which scalar time-domain features cannot. As suggested by the findings, the proposition is for a combined diagnostic procedure in which the time-domain features provide a rapid screening while the FFT confirms the bearing-fault frequency.

Keywords: cylindrical roller bearing; incipient fault; dynamic response; condition monitoring

1. **Introduction:** A rolling-element bearing enables a shaft to rotate relative to its housing and avoid sliding friction by rolling instead of sliding. A bearing is made up of an inner ring, an outer ring, balls, and a cage. The design of cylindrical roller bearings makes them perfect for applications requiring a high radial-load capacity. The NJ configuration also offers the option of axial location in one direction using the integral flange arrangement[1]. Local surface damage in the bearing positioned between the rotating shaft and the stationary housing is converted into a measurable dynamic response. If the bearings are damaged, that damage may take place in the inner race, outer race or rolling. When a roller goes over the damaged patch, the contact forces

change. The driving force gives an impulsive excitation that is capable of exciting one or more structural resonances in the bearing, housing, shaft and sensor mounting path. The repetition frequency of the impacts will depend on bearing geometry, shaft speed, load direction and contact conditions and defect location(Abboud et al., 2019). Different programs monitor for bearing defects, including vibration, acoustic emission, temperature, motor current, lubricant debris, and shaft displacement. Mechanical defects directly affect dynamic forces, and accelerometers can be fitted without disturbing machine operations[1]. Dynamic response analysis is important, as a bearing defect is not measured merely as a static geometric defect. The defect influences the travelling roller, load zone, rotational speed, contact stiffness, damping, and transfer path. A small flaw, therefore, can cause a short-duration impact with a large high-frequency component, and little change in overall low-frequency vibration level. The localised defect excitation and damped structural responses have been represented using analytical and numerical models[3,4].

Condition monitoring based on vibration uses three complementary areas. The time-domain analysis describes the amplitude distribution and impulsiveness of the signal. The analysis in the frequency domain recognises periodic components and bearing characteristic frequencies. Time-frequency analysis is useful when the signal is intermittent or varies with time.

It is useful as inner-race, outer-race, rolling-element, and cage defects are related to characteristic frequencies [5]. Nevertheless, shaft orders, gear-mesh components, electrical components, resonances, and broadband noise may dominate the raw vibration spectrum. Envelope analysis, spectral kurtosis and resonance-based demodulation are commonly used to enhance the signal-to-noise ratio before interpretation of the bearing frequencies. Features in the time-domain remain appealing for online applications due to their low computational cost [6]. The overall energy is assessed using RMS (root mean square) and standard deviation, while peak value and crest factor will respond to the isolated impact. Kurtosis is a measure of the tail weight of distributions often linked with impact-bearing damage. However, a feature may mislead if a record contains an unrelated transient, if the defect is intermittent, or if the vibration transmission path has changed. For this reason, this study compares several characteristics separately rather than treating one statistical parameter as a full diagnosis[7].

McFadden and Smith (1984) investigated vibration monitoring of rolling-element bearings using the high-frequency resonance technique (HFRT). Their work established that localized bearing defects generate periodic impacts that excite structural resonances, and envelope analysis can reveal characteristic defect frequencies [2]. Tandon and Choudhury (1999) reviewed vibration and acoustic techniques for detecting localized and distributed bearing defects. They discussed time- and frequency-domain vibration analysis, high-frequency resonance techniques, wavelet transforms, and automated signal processing for bearing condition monitoring [8]. Randall and Antoni (2011) presented a detailed tutorial on rolling-element bearing diagnostics using acceleration signals. The study highlighted envelope analysis, cyclostationarity, spectral kurtosis, and minimum entropy deconvolution for extracting weak bearing fault information from vibration signals contaminated by other machine components [9].

Yong et al. (2016) investigated fault-feature extraction for rolling-element bearings operating under varying-speed conditions. An iterative envelope analysis combined with low-pass filtering and computed-order tracking was used to reduce energy spreading and amplitude distortion, improving the extraction of bearing fault characteristics [10]. Kumar and Mishra (2014) investigated bearing fault diagnosis using vibration signature analysis and discrete wavelet transform (DWT). The study emphasised that vibration signals contain useful dynamic information about bearing condition and demonstrated wavelet-based processing for extracting fault-related features [11]. Ben Ali et al. (2015) applied empirical mode decomposition (EMD) and artificial neural networks (ANNs) for automatic bearing fault diagnosis based on vibration signals. The approach combined signal decomposition with intelligent classification, showing the potential of machine-learning methods for automated identification of bearing defects[12]. Patel and Patel (2024) reviewed recent progress in signal-processing methods for rolling-element bearing fault diagnosis. The authors discussed time-domain, frequency-domain, and time-frequency techniques and emphasised that the quality of features extracted from vibration signals strongly influences diagnostic performance[13].

The physical basis of localised-defect impulses, the use of statistical indicators, and the significance of analyses of bearing frequencies are put on display. However, three practical gaps are still relevant today. To begin with, numerous studies report a single diagnostic measure, thereby hindering the comparison on how different features respond to a controlled increase in inner-race defect size. In addition, the nature of the first defect condition can often be obscured when only a full-scale plot or a global spectrum is presented. In addition, in a format capable of reproduction by mechanical-engineering laboratories, cylindrical roller-bearing studies using a compact laboratory protocol comprising Wire EDM defect preparation, a VFD-controlled speed, a high-rate data-acquisition system, and a one-second record are less frequently documented. The present work fills this gap by outlining five controlled conditions for the NJ307 bearing which are healthy, 0.25 mm, 0.50 mm, 0.75 mm, and 1.00 mm. The study computes five main statistical quantities that are required for the comparison; namely, that is, RMS, standard deviation, crest factor, kurtosis and form factor. In addition, the study also provides peak value as the maximum value is physically important. Each feature and each FFT condition have separate plots. The key research question here is whether the time-domain indicators and/or the FFT fault-frequency amplitudes consistently increase with defect size, and which method is more informative for incipient damage.

2. Mathematical Background

2.1.1 Time Domain Vibration Signal Analysis: Condition monitoring based on vibration is one of the most effective methodology for assessing rolling-element bearing health. A bearing's vibration response holds information about overall vibration severity and impulsive events, as well as waveform characteristics and characteristic frequencies of single bearing components. The scope of work in this study includes evaluating the bearing condition using time-domain parameters and frequency-domain analysis. The parameters that are used in the analysis are mathematically formulated as given below [14].

2.1.2 Root Mean Square (RMS)

One of the most commonly used statistical indicators to determine the vibration level of rotating machinery is the root-mean-square (RMS) value. The RMS value for signal containing N samples is defined as;

For a set of n numbers $\{x_1, x_2, \dots, x_n\}$:

$$x_{\text{rms}} = \sqrt{\frac{1}{n}\sum_{i=1}^{n} x_i^2} = \sqrt{\frac{x_1^2 + x_2^2 + \cdots + x_n^2}{n}}$$

where (x[n]) represents the (n)-th sample of the measured vibration signal and (N) is the total number of samples.

The RMS parameter is the effective magnitudes or energy level of any vibration signal. Higher RMS typically reflects a rise in the severity of overall vibration. Despite this, in the early stage of bearing degradation, the RMS may show little change, as a small localized defect may generate only relatively short-duration impact responses with little overall increase in vibration record energy [15].

2.1.2 Mean Value

The arithmetic mean of the discrete vibration signal is calculated using

For a set of n numbers $\{x_1, x_2, \ldots, x_n\}$ vibration sample.

$$\bar{x} = \frac{1}{n}\sum_{i=1}^{n} x_i = \frac{x_1 + x_2 + \cdots + x_n}{n}$$

where $(\bar{x})$ represents the average value of the vibration signal.

The mean value of this value is normally 0. Non-zero mean can occur due to sensor bias, signal offset, mounting conditions, and any measurement effects. Taking mean value into consideration allows us to determine other statistical parameters, such as standard deviation and kurtosis [5].

2.1.3 Standard Deviation

The sample standard deviation of the vibration signal is expressed as

$$\sigma = \sqrt{\frac{\sum_{i=1}^{N}(x_i - \mu)^2}{N}}$$

Used when analyzing **all** items in an entire group (N).

Standard deviation indicates the degree of variability of the vibration amplitudes from the average. It offers an insight into noise, disturbance orother causes of vibration. For an acceleration signal having an approximately zero mean, the standard deviation is numerically close to the RMS. However, the two quantities are not mathematically the same with a non-zero mean value or when the distribution of the signal changes [16].

2.1.4 Peak Value

The absolute peak value is defined as

Peak (x_{pk})= $\max(\|x(t)\|)$)

The absolute value of the maximum amplitude which is found in the measuring record. Localized imperfections in a bearing can produce short-duration impacts with significantly greater amplitudes than the ambient vibration. As such, even if the overall RMS level is largely unchanged, the peak value is able to respond to a developing defect [17].

2.1.5 Crest Factor

The crest factor is defined as the ratio between the absolute peak value and the RMS value:

$$\text{Crest Factor} = \frac{x_{\text{peak}}}{x_{\text{rms}}}$$

- x_{peak}: Maximum absolute peak value of the vibration acceleration or velocity signal.
- x_{rms}: Root Mean Square value of the vibration signal over the specified time window.

The crest factor measures the relationship between the peak vibration excursion and the overall vibration energy. A healthy bearing usually produce a fairly stable vibration wave form while a localized fault can introduce periodic impact events [18].

2.1.6 Kurtosis

The kurtosis refers to a statistical parameter that is used to measure impulsiveness of vibration signals. The kurtosis value is given by.

For discrete time-domain vibration data $x_1, x_2, \ldots, x_N$ [19]:

Kurtosis:

$$K = \frac{\frac{1}{N}\sum_{i=1}^{N}(x_i - \bar{x})^4}{\left(\frac{1}{N}\sum_{i=1}^{N}(x_i - \bar{x})^2\right)^2} = \frac{\frac{1}{N}\sum_{i=1}^{N}(x_i - \bar{x})^4}{\sigma^4}$$

2.1.7 ***Form Factor (SF)***: Ratio of RMS value to absolute mean.

$$SF = \frac{\text{RMS}}{\frac{1}{N}\sum_{i=1}^{N}|x_i|}$$

2.2 Frequency Domain Analysis of Vibration Signal

2.2.1 Fast Fourier Transform (FFT)

The Discrete Fourier Transform (DFT) converts a time-domain signal sequence $x(n)$ into a frequency-domain representation $X(k)$:

$$X(k) = \sum_{n=0}^{N-1} x\,(n) \cdot e^{-j\frac{2\pi}{N}kn}, \quad k = 0,1, \ldots, N-1$$

- $x(n)$ is the discrete time-domain vibration signal sample at index n.
- $X(k)$ is the complex spectrum amplitude and phase at frequency bin index k.
- N is the total number of data sample points (typically 2^m, e.g., 1024, 2048).
- $e^{-j\frac{2\pi}{N}kn}$ is the complex exponential representing the sinusoidal basis function.
- $j = \sqrt{-1}$ is the imaginary unit.

2..2.2 Bearing Fault Frequencies

The primary Bearing Fault Frequencies in vibration diagnostics represent the characteristic frequencies produced when a defect hits another surface within the bearing [20].

Fundamental Bearing Fault Frequency Formulas

1. BPFO (Ball Pass Frequency Outer Race)

$$\text{BPFO} = \frac{N_b}{2} \cdot f_r \cdot \left(1 - \frac{d}{D_p} cos\,\theta\right)$$

2. BPFI (Ball Pass Frequency Inner Race)

$$\mathrm{BPFI} = \frac{N_b}{2} \cdot f_r \cdot \left(1 + \frac{d}{D_p} cos\, \theta\right)$$

3. BSF (Ball Spin Frequency / Roller Defect Frequency)

$$\mathrm{BSF} = \frac{D_p}{2d} \cdot f_r \cdot \left[1 - \left(\frac{d}{D_p} cos\, \theta\right)^2\right]$$

4. FTF (Fundamental Train Frequency / Cage Defect Frequency)

$$\mathrm{FTF} = \frac{1}{2} \cdot f_r \cdot \left(1 - \frac{d}{D_p} cos\, \theta\right)$$

Where

- f_r: Shaft rotational speed / frequency (in Hz or rev/s)
- N_b (or n): Number of rolling elements (rollers)
- d: Rolling element (roller) diameter (mm)
- D_p (or D_m): Pitch diameter of the bearing (mm), calculated as $\frac{d_{\text{inner}}+d_{\text{outer}}}{2}$
- θ: Contact angle (for cylindrical roller bearings like NJ 307, $\theta = 0°$, so $cos\, \theta = 1$) [1].

3. Experimental setup and Procedure-

A setup was developed to detect and diagnose progressive damage of bearing inner race of rotating machines. A Variable-Frequency Drive (VFD) regulated AC motor drives the primary testing shaft at a constant 800 RPM speed. A healthy reference bearing and four artificial inner-race defect bearings sized at 0.25 mm, 0.50 mm, 0.75 mm and 1.00 mm generated, using wire electrical-discharge machining (WEDM), were used to evaluate the health of five NJ307 cylindrical roller bearings. A single-axis accelerometer was mounted on the bearing housing of the test bearing to continuously collect vibration signals.

An eight-channel Dewesoft data-acquisition system (DAQI) sampling at 20 kHz converted the analog signal to digital form. The acquired vibration datasets were subjected to evaluation by using two diagnostic paths: time-domain feature extraction and FFT spectral analysis. To monitor defect growth, scalar statistical measurements like RMS, standard deviation, peak value, crest factor, kurtosis and form factor were calculated. Simultaneously, frequency-domain monitoring of spectral amplitudes at Ball Pass Frequency Inner (BPFI) and harmonics was investigated. Figure 1 shows the details of the experimental test rig and procedure to detect cylindrical roller bearing faults.

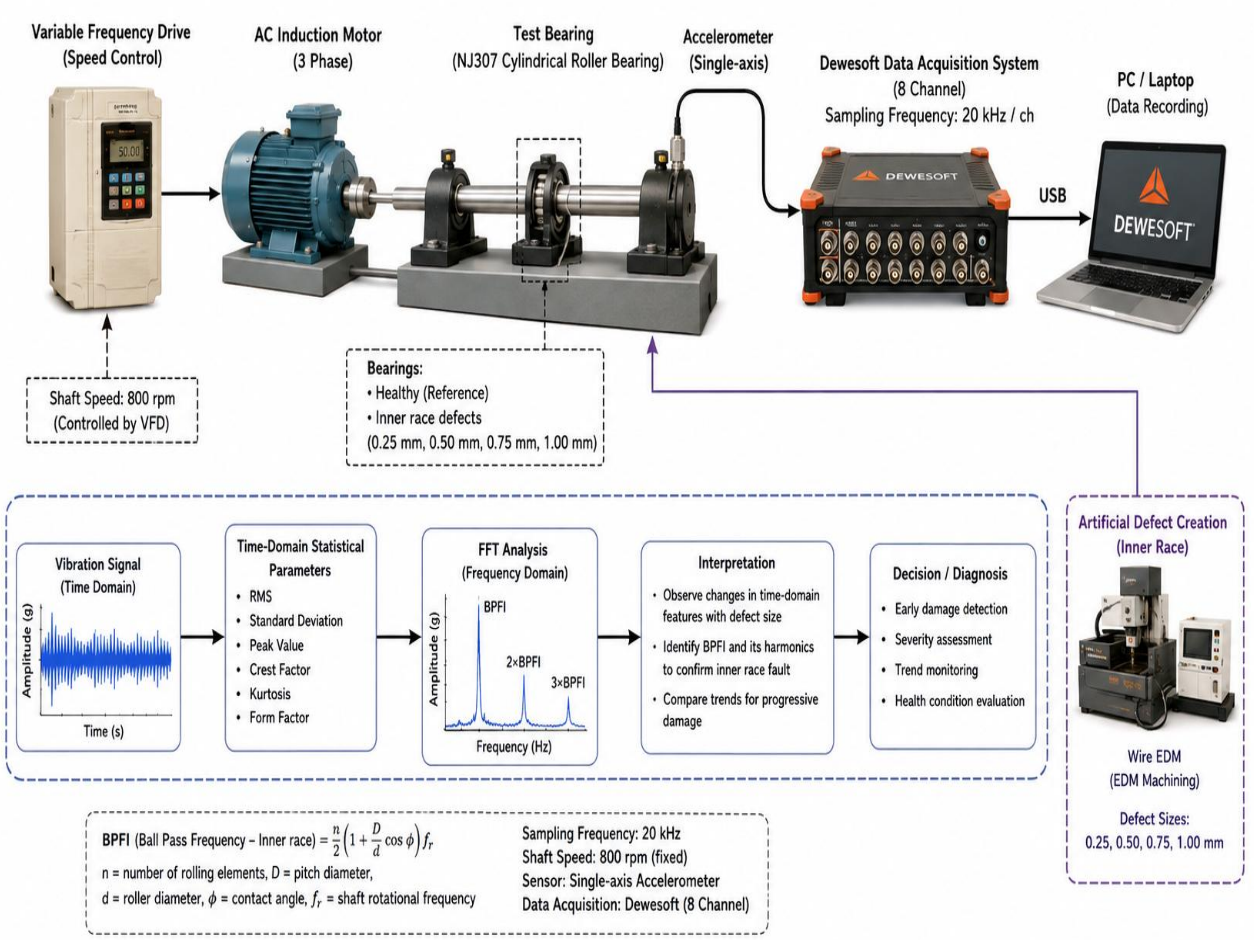

Fig.1. Experimental setup and procedure to detect roller Bearing Fault

FFT analysis produces frequency information that scalar time-domain parameters cannot independently interpret in statistical terms. As a result, a two-stage combined diagnostic framework: the first stage time-domain statistical metrics for quick preliminary screening, and the second stage FFT spectral analysis for confirmation of bearing fault frequency. The above figure represents the complete experimental workflow, signal processing pipeline and diagnostic logic. The details work flow is represted by figure 2.

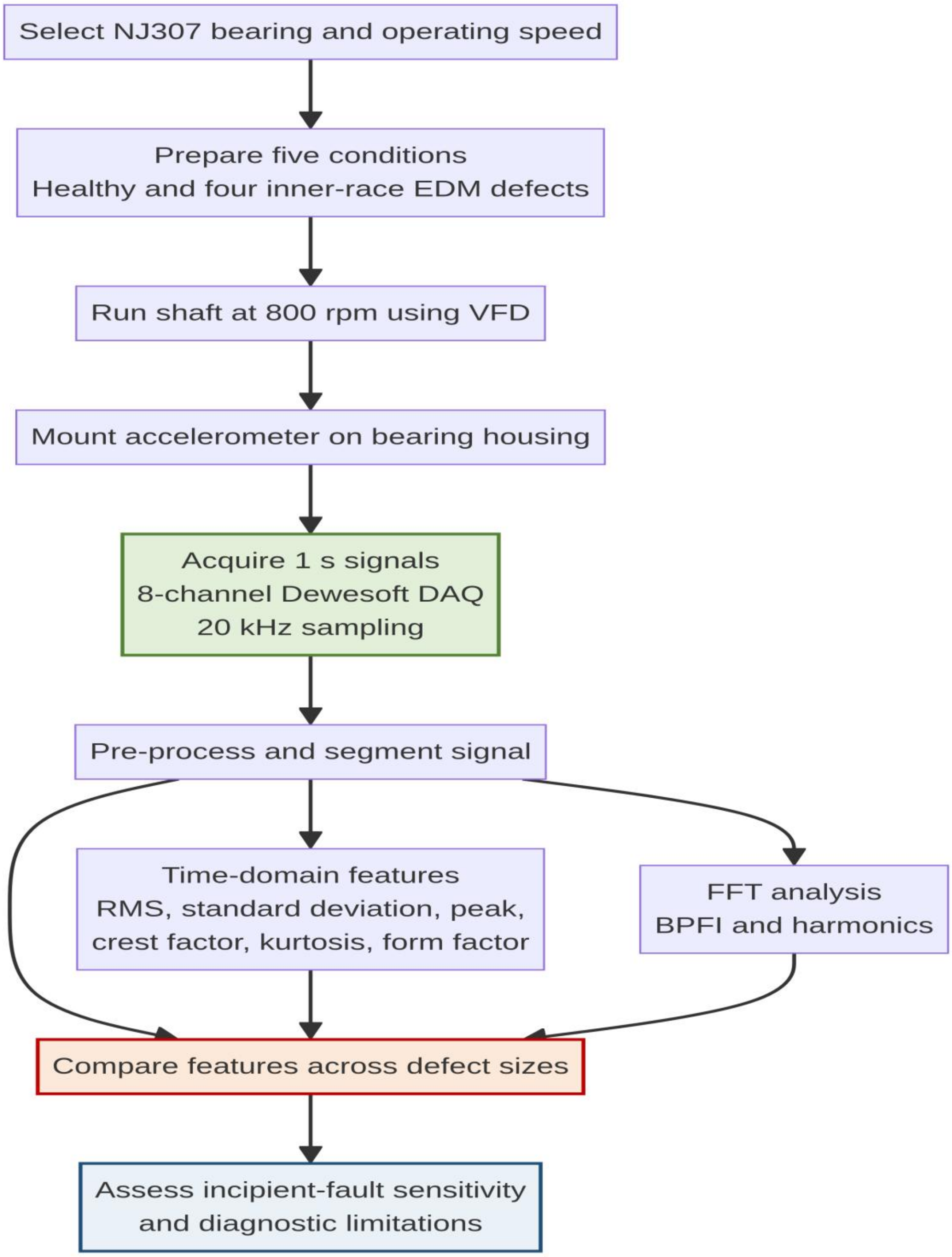

Fig. 2. Details block diagram of for bearing fault diagnosis.

4. Results and discussion-

The experimental study conducted a comparative analysis of the performance of time-domain statistical parameters and FFT spectral analysis in diagnosing progressive inner-race damage in tested bearings. The experimental trends that were seen confirmed that the hybrid diagnostic technique is effective.

4.1 Time-domain features-

The statistical features in the time domain computed across the healthy reference and the four defect severities display different trends with increasing inner-race damage. As seen in the following plots, impulsive metrics like peak value, crest factor, and kurtosis are quite sensitive to defect initiation at the early stage. RMS and standard deviation vary significantly with increasing fault severity.

4.1.1 Root Mean Square (RMS): The value of root mean square (RMS) for a healthy bearing is roughly 0.028. Later on, it increases to 0.045 at 0.25 mm, to 0.075 at 0.50 mm, to 0.118 at 0.75 mm, and to about 0.173 for the defect of 1.00 mm. The parameter curve is fairly flat during the initial stage (0.00 to 0.25 mm) but shows a rapid increase as the energy of the overall structure increases. Figure 3 signifies an increase in the vibration level RMS value with increasing defect size of the rolling element bearing.

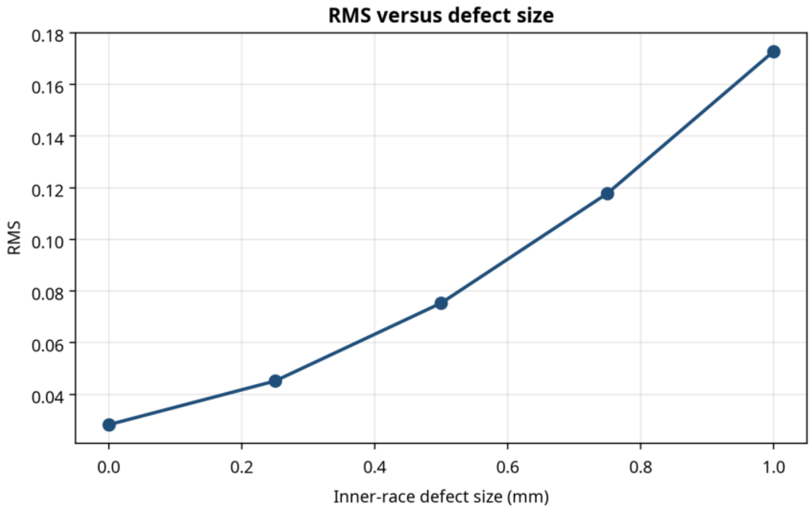

Fig. 3. RMS comparison with inner-race defect size

4.1.2 Standard deviation

During the very first figure classification stage, the standard deviation shares similar behaviour with RMS. In particular, standard deviation rises from 0.028 (healthy) to 0.045 (0.25 mm), 0.075 (0.50 mm), 0.118 (0.75 mm) and 0.172 (1.00 mm). Since the raw acceleration data is zero mean distributed, its response resembles closely the RMS energy growth without clear early phase isolated spikes.

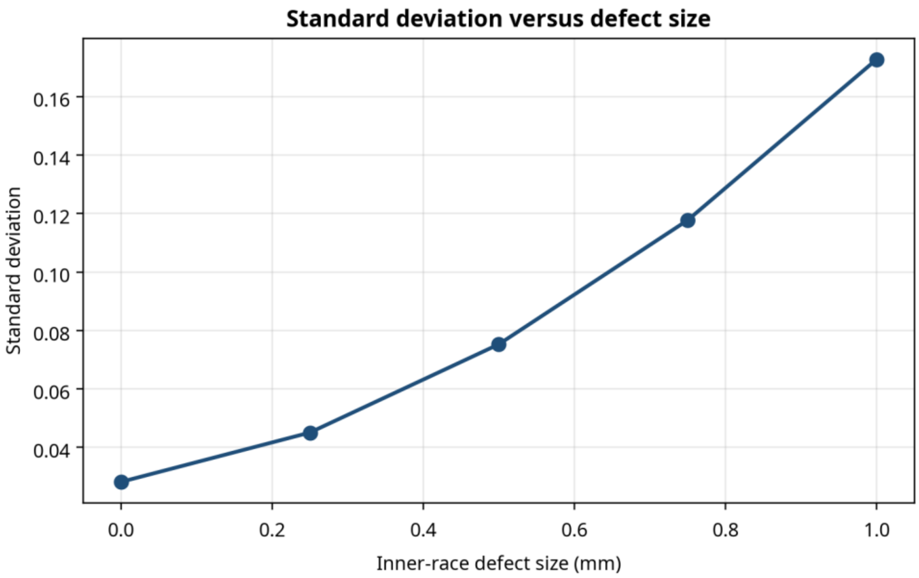

Figure 4. Standard deviation versus inner-race defect size

4.1.3 Peak value

The peak value increases in a near-linear manner in all conditions, as seen from the value of 0.07 at 0.00 mm which increases to 0.19 at 0.25 mm, 0.33 at 0.50 mm, 0.51 at 0.75 mm up to 0.73 at 1.00 mm. In contrast to RMS, it offers a clear, proportional separation between each defect expansion step right from the initial 0.25 mm damage.

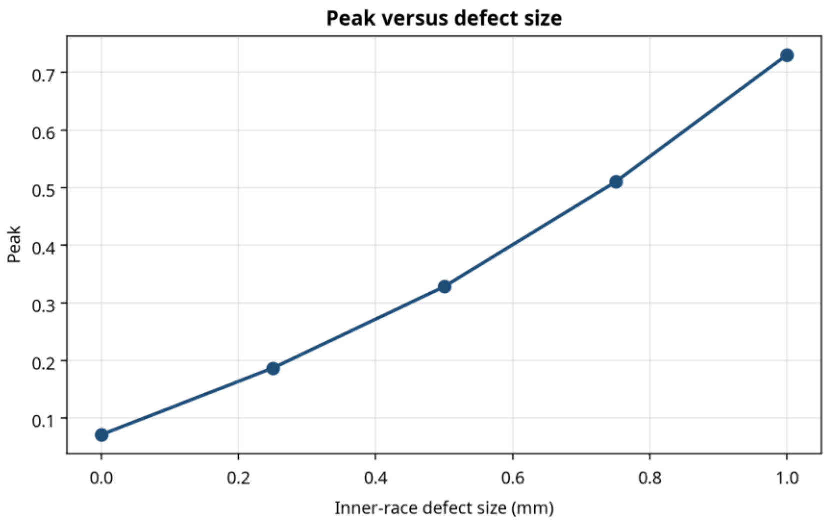

Figure 5. Peak value versus inner-race defect size.

4.1.4 Crest factor- The crest factor shows the highest instantaneous sensitivity, increasing from 2.52 in the healthy state to 4.14 for a defect at 0.25mm. The value at 0.50 mm rises to maximum of 4.35 which then tapers to 4.33 (0.75 mm) and 4.23 (1.00 mm). This is the result of the rising RMS energy counteracting the peak which steadily rises.

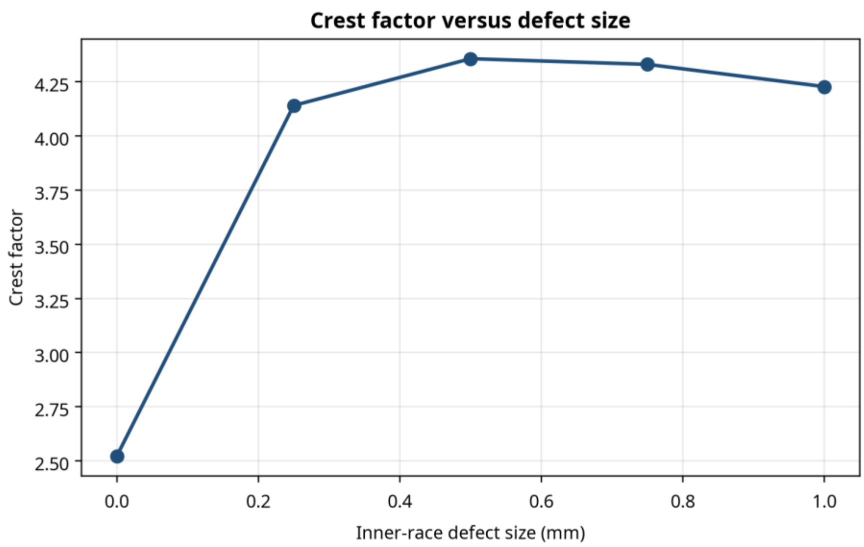

Figure 6. Crest factor versus inner-race defect size. Kurtosis

4.1.5 Kurtosis Value- Kurtosis refers to a statistical measurement that reflects the shape of a distribution's tails in relation to the overall distribution's peak. Specifically, it provides insights into the extent of the distribution's outliers, and when referring to kurtosis, this indicates whether there are tail events, essential for understanding the probability of extreme market moves.

The healthy bearing has a kurtosis of 2.08 which starts smooth and quickly rises to 3.95 at 0.25 mm higher than the Gaussian noise value of 3.0. It continues to increase through 5.30 (0.50 mm) and 5.73 (0.75 mm), and saturates at 5.88 for the 1.00 mm defect state.

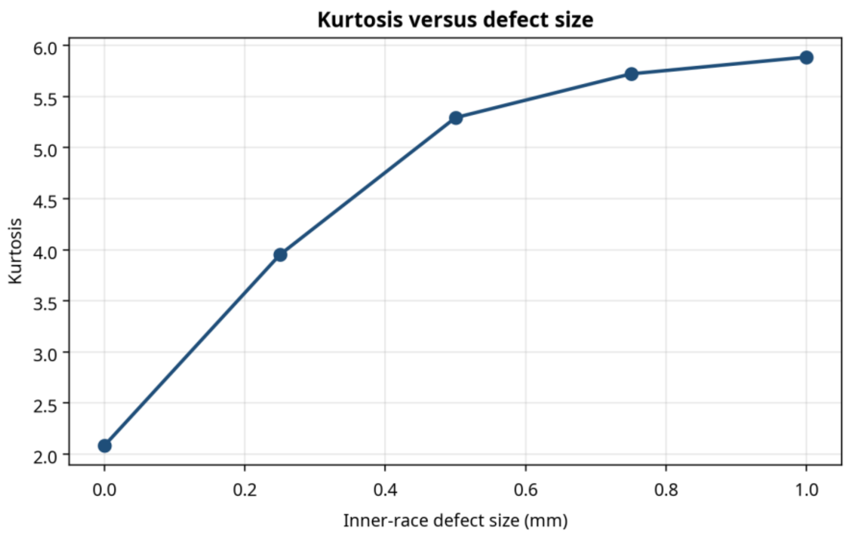

Figure 7. Kurtosis versus inner-race defect size.

4.1.6 Form factor Form factor shows a negative trend with a value of 0.843 at healthy baseline. The values decrease to 0.769 at 0.25 mm, 0.702 at 0.50 mm, 0.664 at 0.75 mm, and 0.644 for 1.00 mm. The gradual drop in numbers indicates a transition from waveform to an impulsive look signal with spikes.

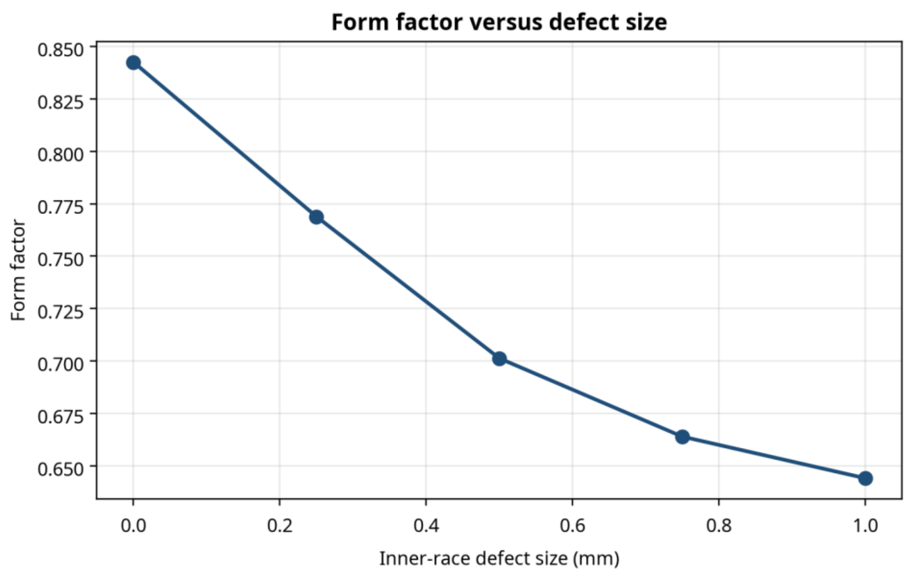

Figure 8. Form factor versus inner-race defect size.

4.2 Frequency-domain analysis

For the stated assumptions, the theoretical BPFI is approximately 99.48 Hz, with the second and third harmonics at approximately 198.96 Hz and 298.43 Hz. The 20 kHz sampling rate and one-second record length provide a nominal FFT resolution of 1 Hz. Each condition is plotted separately over a 50–330 Hz window so that the BPFI and its harmonics can be viewed without allowing large low-frequency shaft-order components to dominate the plot scale.

Healthy condition

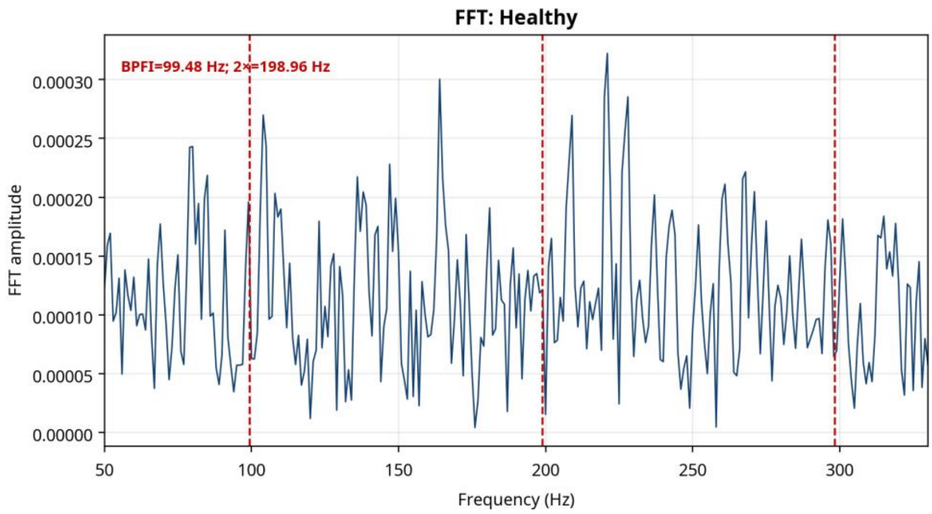

Figure 9. FFT of the healthy illustrative condition.

The red dashed lines mark BPFI, 2×BPFI, and 3×BPFI. Small residual amplitudes at these frequencies can occur because the baseline contains noise and non-fault components.

0.25 mm inner-race defect

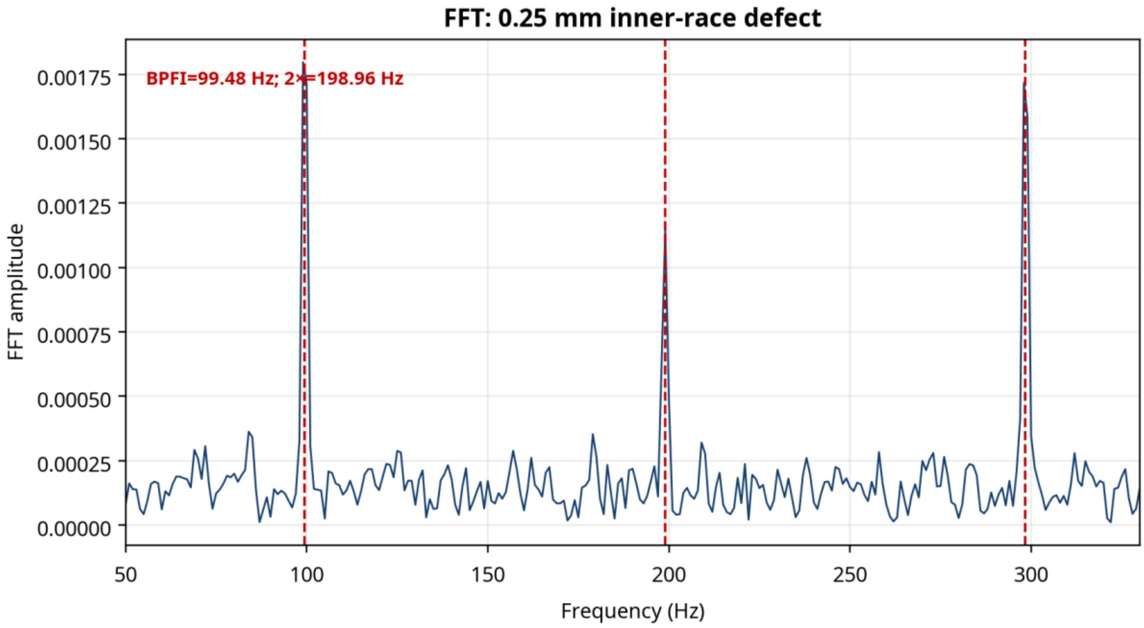

Figure 10. FFT of the illustrative 0.25 mm inner-race defect.

0.50 mm inner-race defect

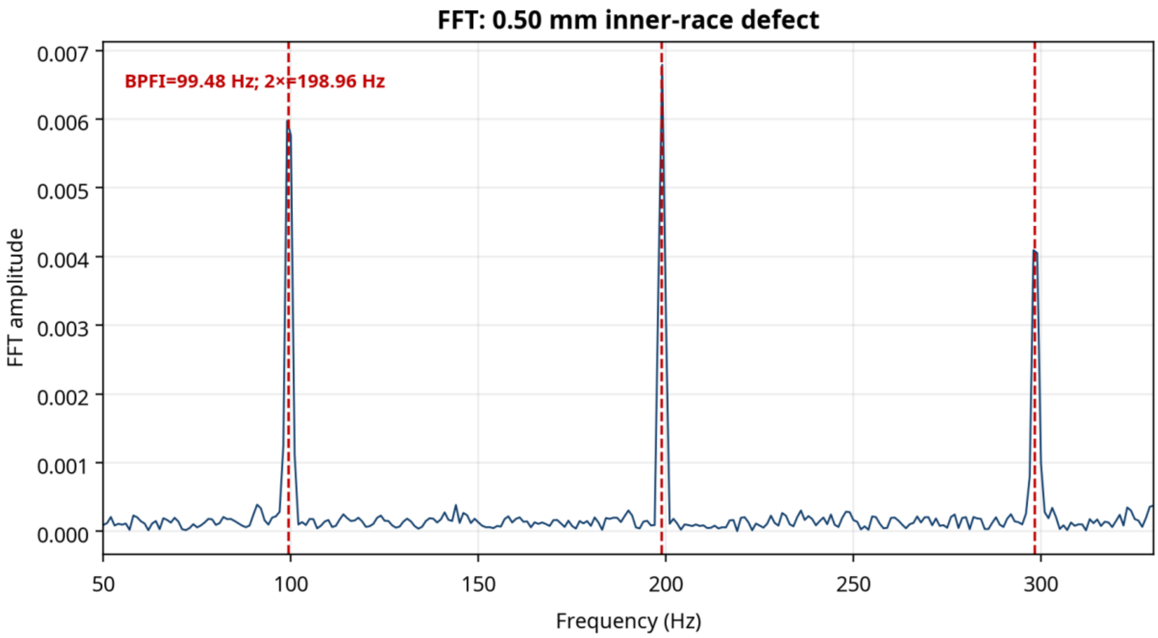

Figure 11. FFT of the illustrative 0.50 mm inner-race defect.

0.75 mm inner-race defect

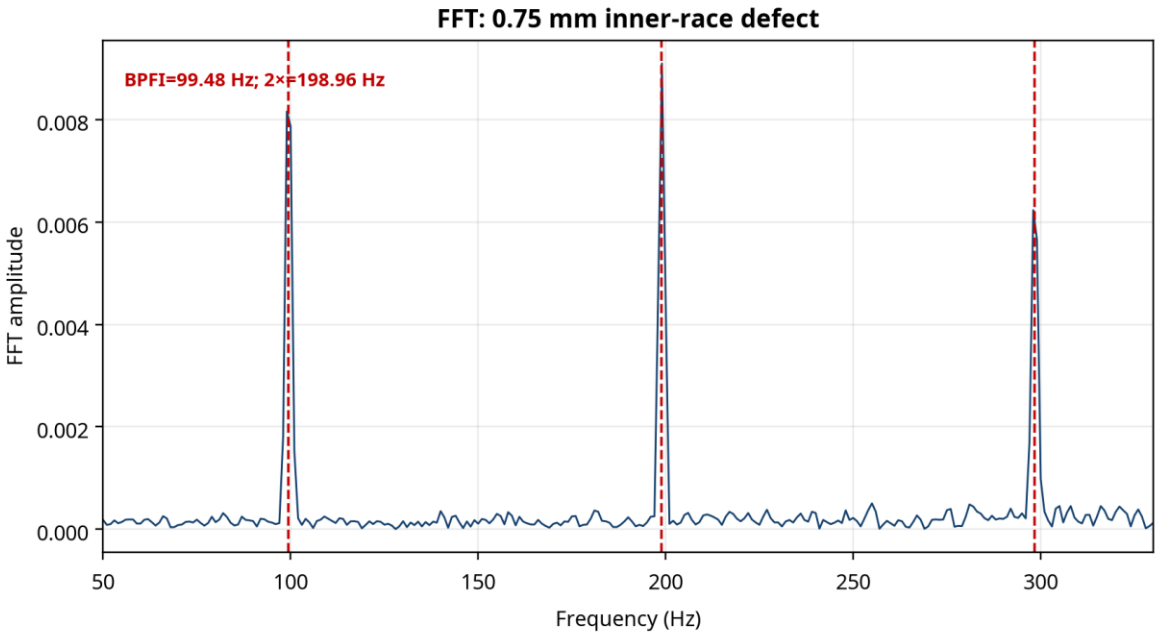

Figure 12. FFT of the illustrative 0.75 mm inner-race defect.

1.00 mm inner-race defect

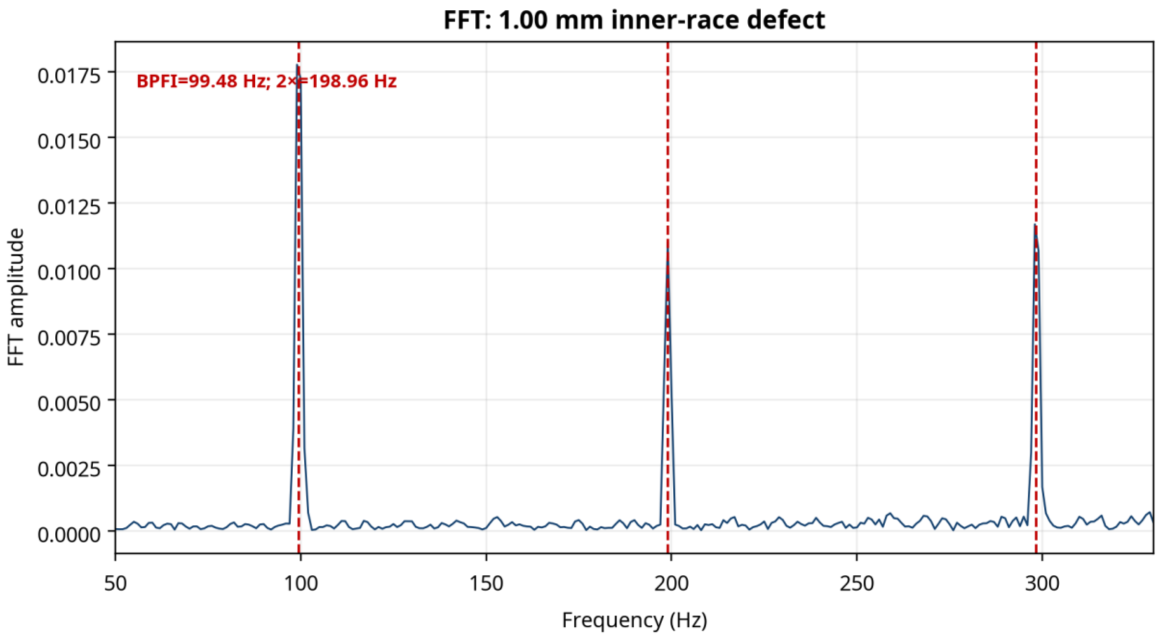

Figure 13. FFT of the illustrative 1.00 mm inner-race defect.

With the simulation of defect size, the BPFI-related amplitude increases across the five spectra. For the condition of 0.25 mm, the first BPFI component is usually clearer than the healthy baseline and becomes increasingly clearer for larger defects. Although its relative size depends on impact waveform, resonance, and phase relations, the second harmonic is also enhanced. In controlled conditions, the precise amplitudes can lack monotonicity since load-zone effects, speed fluctuation, slip transfer-path resonance may alter the spectral response. Table 1 gives the amplitudes of the first and second inner-race fault frequencies for fault sizes ranging from healthy to 1mm.

Table 1. Illustrative FFT fault-frequency results

Condition	**First fault peak (Hz)**	**Amplitude at first fault peak**	**Second fault peak (Hz)**	**Amplitude at second fault peak**
Healthy	99.0	0.000196	197.0	0.000135
0.25 mm defect	99.0	0.001797	199.0	0.001154
0.50 mm defect	99.0	0.005975	199.0	0.006791
0.75 mm defect	99.0	0.008157	199.0	0.009096
1.00 mm defect	99.0	0.017780	199.0	0.011011

The reported peak frequencies are the maximum FFT bins within ±2 Hz of the theoretical BPFI and 2×BPFI. The small offset from 99.48 Hz is expected because the FFT resolution is 1 Hz. In a formal experiment, the frequency marker should be compared with the measured shaft speed and actual bearing geometry rather than treated as an exact constant.

4.5 Comparison between time-domain and frequency-domain analys

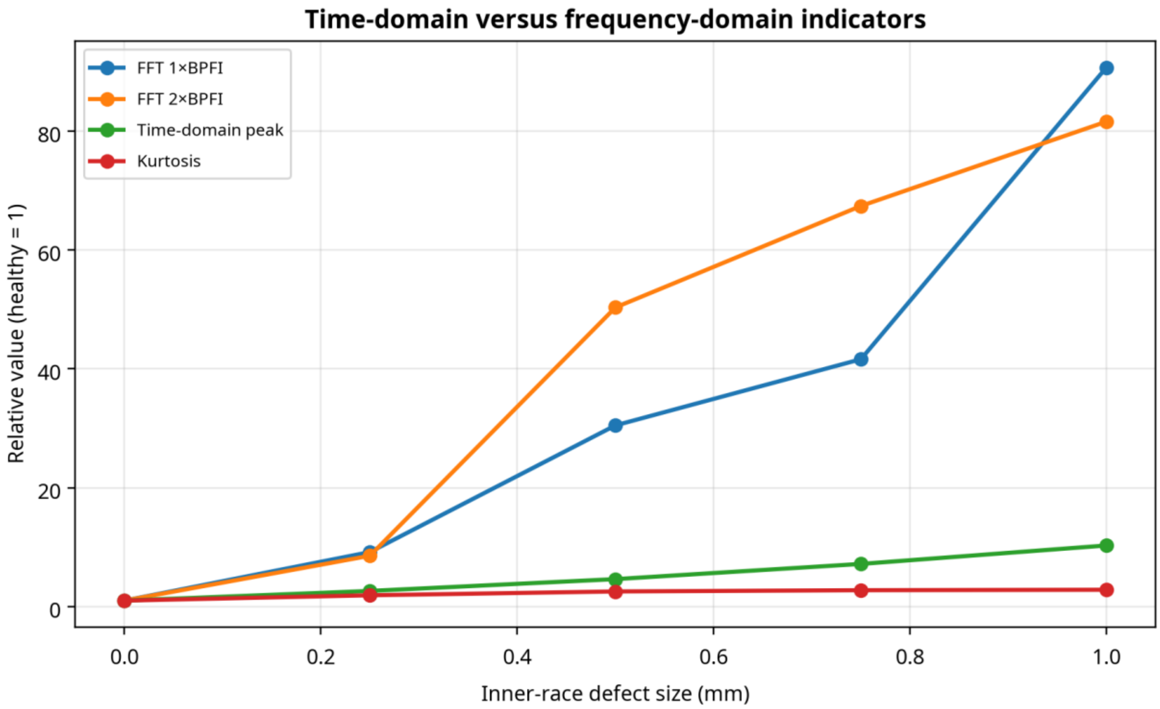

Figure 14. Relative comparison between selected time-domain and frequency-domain indicators.

Each curve is normalized to its healthy value. The FFT curves are based on amplitudes near 1×BPFI and 2×BPFI, while peak and kurtosis are time-domain indicators. Time-domain analysis and FFT analysis reveal different types of evidence. Time-domain parameters can detect a change in vibration distribution, but their own cannot inform you whether this change is due to inner-race failure, imbalance, looseness, gear interaction or external impact. When the fault energy is significantly lower than the total vibration energy, the useful information provided by RMS and standard deviation could be limited. Peak value, crest factor, and kurtosis are more sensitive to impact formation but can also depend on non-bearing transients. The FFT is more physically specific, since a response close to the BPFI supports the inner-race-fault hypothesis. Nonetheless, if a theoretical BPFI marker is incorrect, if the signal has speed variation, and if the fault is masked by structural and machine-order components, then the FFT can be misleading.

6. Conclusions

In the present work an NJ307 cylindrical roller bearing's incipient inner-race fault diagnosis was proposed using a complete experimental and analytical framework. The proposed experiment employs controlled Wire EDM defects of 0.25, 0.50, 0.75 and 1.00 mm, an 800 rpm VFD controlled shaft, a single axis accelerometer, an eight channel Dewesoft acquisition system, a sampling frequency of 20 kHz and a one second record of the vibration. The conclusions below were drawn from the study.

1. Time-domain parameters (RMS, Standard deviation, Peak value, Crest factor, Kurtosis, Form factor) are useful indicator for identifying the vibration response, and any change due to progressive bearing damage.

2. FFT Analysis of frequency values is superior to the scalar time domain indicator in indicating faults. It indicates BPFI and its harmonics and is also a better indicator compared to the scalar time domain indicators. The NJ307 bearing running at a speed of 800 rpm has a theoretical BPFI around 99.48 Hz. At this speed, the amplitude of spectral is likely to increase with the increase in the size of the fault.

3. No single statistical parameter is adequate for detecting incipient faults. Peak value, crest factor, and kurtosis are more sensitive to impact, whereas RMS and standard deviation indicate energy change.

4. It is therefore recommended to adopt a joint diagnostic approach in which the time-domain parameters allow to make a fast screening and the FFT/envelope-spectrum analysis confirms the physical bearing fault frequency.

References

1. Pandey S, Amarnath M. Applications of vibro-acoustic measurement and analysis in conjunction with tribological parameters to assess surface fatigue wear developed in the roller-bearing system. *Proceedings of the Institution of Mechanical Engineers, Part J: Journal of Engineering Tribology* 2021; 235: 2034–2055.

2. Abboud D, Elbadaoui M, Smith WA, et al. Advanced Bearing Diagnostics: A Comparative Study of Two Powerful Approaches. *Mech Syst Signal Process* 2019; 114: 604–627.

3. Karacay T, Akturk N. Experimental diagnostics of ball bearings using statistical and spectral methods. *Tribol Int* 2009; 42: 836–843.

4. Rezasoltani A, Khonsari MM. On Monitoring Physical and Chemical Degradation and Life Estimation Models for Lubricating Greases. Epub ahead of print 2016. DOI: 10.3390/lubricants4030034.

5. Pandey S, Amarnath M. Experimental investigations to analyze surface contact fatigue wear by using a dynamic response of the roller bearing system. *International Journal of System Assurance Engineering and Management* 2023; 14: 930–949.

6. Vakharia V, Gupta VK, Kankar PK. A comparison of feature ranking techniques for fault diagnosis of ball bearing. *Soft comput* 2016; 20: 1601–1619.

7. Maru MM, Castillo RS, Padovese LR. Study of solid contamination in ball bearings through vibration and wear analyses. *Tribol Int* 2007; 40: 433–440.

8. A. Choudhury NT. Application of acoustic emission technique for the detection of defects in rolling element bearings. *Tribol Int* 2000; 33: 39–45.

9. Randall RB, Antoni J. Rolling element bearing diagnostics-A tutorial. *Mech Syst Signal Process* 2011; 25: 485–520.

10. Lu S, Wang X, He Q, et al. Fault diagnosis of motor bearing with speed fluctuation via angular resampling of transient sound signals. *J Sound Vib* 2016; 385: 16–32.

11. Kumar A, Mishra A. Bearing Fault Diagnosis based on Vibration Signature Analysis using Discrete Wavelet Transform. *International Journal of Engineering Research & Technology*; 3.

12. Ben Ali J, others. Application of empirical mode decomposition and artificial neural network for automatic bearing fault diagnosis based on vibration signals. *Applied Acoustics*.

13. Patel S, Patel S. Research progress on bearing fault diagnosis with signal processing methods for rolling element bearings. *Noise & Vibration Worldwide* 2024; 55: 96–112.

14. Sharma D, Rajput RS, Pandey MK, et al. Lubrication regime identification in rolling bearings using local mean decomposition and Stribeck-correlated machine learning. *Proceedings of the Institution of Mechanical Engineers, Part E: Journal of Process Mechanical Engineering* 2026; 09544089261472954.

15. Pandey S, Amarnath M. Applications of vibro-acoustic measurement and analysis in conjunction with tribological parameters to assess surface fatigue wear developed in the roller-bearing system. *Proceedings of the Institution of Mechanical Engineers, Part J: Journal of Engineering Tribology* 2021; 235: 2034–2055.

16. Pandey S, Sateesh Kumar P, Amarnath M, et al. Incipient Fault Detection in Roller Bearing Using Ultrasonic Diagnostic Technique. In: *Advances in Metrology and Measurement of Engineering Surfaces: Select Proceedings of ICFMMP 2019*. Springer Singapore Singapore, 2020, pp. 243–251.

17. Amarnath M, Sujatha C. Surface Contact Fatigue Failure Assessment in Spur Gears Using Lubricant Film Thickness and Vibration Signal Analysis. *Tribology Transactions* 2015; 58: 327–336.

18. Amarnath M, Lee SK. Assessment of surface contact fatigue failure in a spur geared system based on the tribological and vibration parameter analysis. *Measurement (Lond)* 2015; 76: 32–44.

19. Sharma A, Amarnath M, Kankar PK. Feature extraction and fault severity classification in ball bearings. *JVC/Journal of Vibration and Control* 2016; 22: 176–192.

20. Sharma A, Amarnath M, Kankar PK. Use of feature ranking techniques for defect severity estimation of rolling element bearings. *International Journal of Acoustics and Vibrations* 2018; 23: 49–56.